4466–4474 *Nucleic Acids Research, 2005, Vol. 33, No. 14*
doi:10.1093/nar/gki750

Kinetic resolution of bimolecular hybridization versus intramolecular folding in nucleic acids by surface plasmon resonance: application to G-quadruplex/duplex competition in human *c-myc* promoter

Kangkan Halder and Shantanu Chowdhury*

Institute of Genomics and Integrative Biology, CSIR, Mall Road, Delhi 110007, India

Received April 4, 2005; Revised May 19, 2005; Accepted July 18, 2005

ABSTRACT

The human oncogene *c-myc* is regulated by G-quadruplex formation within the nuclease hypersensitive element (NHE III$_1$) in the *c-myc* promoter, making the quadruplex a strong anti-cancer target. With respect to this, the competing equilibrium between intramolecular quadruplex folding and bimolecular duplex formation is poorly understood and very few techniques have addressed this problem. We present a method for simultaneously determining the kinetic constants for G-quadruplex folding/unfolding and hybridization in the presence of the complementary strand from a single reaction using an optical biosensor based on surface plasmon resonance (SPR). Using this technique, we demonstrate for the first time that quadruplex formation in the *c-myc* promoter is favored at low strand concentrations. Our results indicate favorable quadruplex folding (equilibrium folding constant K_F of 2.09 calculated from the kinetic parameters: folding rate constant, $k_f = 1.65 \times 10^{-2}\,s^{-1}$ and unfolding rate constant, $k_u = 7.90 \times 10^{-3}\,s^{-1}$) in 150 mM K^+. The hybridization rate constants detected concurrently gave a bimolecular association constant, $k_a = 1.37 \times 10^5\ M^{-1}\ s^{-1}$ and dissociation constant, $k_d = 4.94 \times 10^{-5}\ s^{-1}$. Interestingly, in the presence of Na^+ we observed that G-quadruplex folding was unfavorable ($K_F = 0.54$). Implication of our results on the *c-myc* transcription activation model is discussed in light of aberrant *c-myc* expression observed on destabilization of the G-quadruplex.

INTRODUCTION

Expression of the oncogene *c-myc* is associated with cellular proliferation and control of differentiation. As a result, loss of regulation resulting in overexpression of *c-myc* is correlated with a large number of human and animal cancers (1–4). Antisense oligonucleotide mediated transcription silencing has been observed to induce differentiation in myelocytes indicating the role of aberrant *c-myc* overexpression in differentiation (5,6). Transcription regulation of *c-myc* is complex and involves multiple promoters, P1 and P2 being prominent among them [for reviews see (4,7)]. The nuclease hypersensitive element (NHE III$_1$), corresponding to −147 to −117 bases relative to P1 transcription initiation site controls >80% of *c-myc* transcription and hence is an important anti-cancer target (8–11). It has been observed that the purine-rich anti-sense strand of the NHE adopts a G-quadruplex conformation and it was recently shown that the structure could be a regulatory switch for *c-myc* (12,13). Based on this and various other observations, postulated models of regulatory control entail a switch between the G-quadruplex and the duplex DNA, which could be central in elucidation of the mechanism of *c-myc* transcription and design of antisense therapy (8,9,11,14). The orchestration of the structural transitions driving this quadruplex–duplex competition is poorly understood.

The G-quadruplex constitutes a four-strand fold-back structure of stacked guanine-tetrads. These tetrads are coplanar arrangement of four guanines held together by Hoogsteen hydrogen bonds (15,16). Apart from the promoter region of *c-myc*, sequences that form G-quadruplex *in vitro* have been found in the telomeres (17) and within the switch regions of immunoglobin heavy-chain genes (18). Interestingly, recent evidence implicates these unusual DNA structures as 'at risk motifs' (19) owing to their involvement in genome rearrangements induced by polymerase slippage events in the nematode *Caenorhabditis elegans* on inactivation of a putative helicase, DOG-1 (20). In a genomic context, formation of G-quadruplex competes with duplex formation and thus the kinetics and thermodynamics of the structural transitions would be the underlying factors determining its functional role.

*To whom correspondence should be addressed. Tel: +91 11 2766 6157; Fax: +91 11 2766 7471; Email: shantanuc@igib.res.in

Determination of the competing rate constants (G-quadruplex folding and hybridization) requires simultaneous determination of the folding/unfolding rates and the duplex formation rates. Nanomotors have been designed based on the folding/unfolding of G-quadruplex motifs, which were demonstrated using FRET (21). The rates of folding/unfolding determined the efficiency of the nanomachine and could be regulated using a duplex trap. A FRET-based study has been used to observe the quadruplex folding constants in the presence of a PNA trap, where the PNA strand concentration was maintained such that hybridization was very fast (22). However, *in vivo* extrapolations can be made only when the strand concentrations are equimolar and very low. A recent report addresses this problem using human telomeric G-quadruplex hybridization on an optical biosensor based on surface plasmon resonance (SPR) and suggests a possible quadruplex–duplex competition mechanism at low equimolar concentration of the complementary strand (23).

Based on DNase I hypersensitivity, it was reported that the major regulatory element of *c-myc* exists in a strand-separated form rendering this location as a NHE III_1 (8). We hypothesized that the underlying inherent kinetics of duplex formation may play a significant role, in conjunction with other cellular factors, which could be important for the crucial regulatory mechanism. In this study, we used SPR-based biosensor to observe competing hybridization versus G-quadruplex formation in the *c-myc* regulatory region at physiological conditions. Using an analytical component resolution method described here for the first time, we could not only simultaneously determine the individual rate constants of folding/unfolding (of G-quadruplex) and association/dissociation (of hybridization) but we also separated the two components of the hybridization reaction. One resulting from hybridization with pre-equilibrated unstructured oligonucleotides present on sensor surface and the other owing to hybridization with immobilized molecules unfolding in the presence of the complementary strand (during injection). We observed that both the folded and the unfolded forms have short half-lives of <90 s and our results further indicated that the rate-limiting step changes as a result of complementary strand concentration. At low-strand concentration hybridization is slow and determines the overall rate while with increasing concentration motif transition becomes rate determining. Based on our results we conclude that G-quadruplex may be the predominant state at the low intracellular strand concentrations because duplex formation is kinetically unfavorable.

Kinetic analysis

A brief introduction to the equations used in the kinetic analysis is summarized here (for details of mathematical derivation see Supporting Information). The applied method is based on SPR applied to an optical biosensor (from BIAcore Inc.), which enables real time detection of molecular association and dissociation reactions by monitoring change in refractive index owing to alteration in mass on the optical sensor (24,25). The refractive index change is represented as response units (RUs) in a sensorgram, which is proportional to the amount of analyte (injected in mobile phase) binding to ligand immobilized on the sensor surface. The basic method and the theoretical background have been described in detail previously (26–28). In SPR biosensor, the interaction between the surface immobilized ligand (A) and the solution phase analyte (B) can be described as follows:

$$\mathrm{A} + \mathrm{B} \underset{k_\mathrm{d}}{\overset{k_\mathrm{a}}{\rightleftharpoons}} \mathrm{A} \bullet \mathrm{B}, \qquad \mathbf{1}$$

where k_a and k_d are the association and dissociation rate constants, respectively, and A•B represents the bound complex formed on the biosensor surface. The kinetic expression for the above type of general ligand–analyte interaction is given by (28)

$$R_{t(\mathrm{assoc})} = \frac{Ck_\mathrm{a}R_\mathrm{max}\left(1-\mathrm{e}^{-(k_\mathrm{a}C+k_\mathrm{d})(t-t_0)}\right)}{(k_\mathrm{a}C+k_\mathrm{d})} + R_\mathrm{i} \qquad \mathbf{2}$$

for the association phase and

$$R_{t(\mathrm{diss})} = R_\mathrm{a}\mathrm{e}^{-k_\mathrm{d}t} + R_{(t\to\infty)} \qquad \mathbf{3}$$

for the dissociation part of the sensorgram, where R_t is the actual observed signal expressed in RU at any time t, R_max is the expected maximal response proportional to the immobilized ligand, C is the constant concentration of analyte in solution, R_i is a fitting parameter equivalent to the signal at the point of injection of analyte ($t = 0$) and accounts for any change in the running buffer composition, R_a is defined as the amplitude of the dissociation curve and $R_{(t\to\infty)}$ is the response value after infinite time and represents complete dissociation of the complex. The rate constants, k_a and k_d, are determined by fitting the sensorgrams to Equations 2 and 3.

Although the above Equations 2 and 3 hold good for any general 1:1 interaction, they cannot account for the presence of an additional equilibrium on the sensor surface. We propose a coupled-kinetic model for this purpose, which simultaneously determines the rate constants for the equilibrium between different conformations of the surface-attached ligand and its interaction with the analyte in mobile phase. We have considered the surface equilibrium as inter-conversions between two possible conformations of the ligand in its immobilized form, where only one of the conformations can interact with the analyte. So, the surface equilibrium could be expressed as follows:

$$F \underset{k_\mathrm{f}}{\overset{k_\mathrm{u}}{\rightleftharpoons}} U, \qquad \mathbf{4}$$

where k_u and k_f are the unfolding and folding rate constants of folded conformation F and the unfolded isoform U of the immobilized ligand, respectively. On considering that analyte can only interact with the unfolded isoform U, the coupled-kinetic model may be represented as follows:

$$F \underset{k_\mathrm{f}}{\overset{k_\mathrm{u}}{\rightleftharpoons}} U,$$

$$U + C \underset{k_\mathrm{d}}{\overset{k_\mathrm{a}}{\rightleftharpoons}} D, \qquad \mathbf{5}$$

where C is the analyte and D the ligand–analyte complex, k_d is the rate constant for dissociation of the complex and k_a represents the bimolecular rate constant of association. In our case, U and F represent the unfolded and folded forms of the G-quadruplex formed by immobilized G1B on sensor

Table 1. Oligonucleotides used in this study

C1	5′-CCCCACCTTCCCCACCCTCCCCACCCTCCCC-3′
G1	5′-GGGGAGGGTGGGGAGGGTGGGGAAGGTGGGG-3′
C1B	biotin-5′-ACGTACGTCCCCACCTTCCCCACCCTCCCCACCCTC-CCC-3′
G1B	biotin-5′-ACGTACGTGGGGAGGGTGGGGAGGGTGGGGAAGGTGGGG-3′
M1	5′-CC**T**CACCTTCCCCACCCTCCCCACCCTCCCC-3′
M2	5′-CCCCACCTTCC**T**CACCCTCCCCACCCTCCCC-3′
M3	5′-CCCCACCTTCCCCACCCTCC**T**CACCCTCCCC-3′

The 31mer oligonucleotides C1 and G1 constitute the NHE the in *c-myc* promoter region corresponding to −147 to −117 bases relative to P1 transcription initiation site. Biotinylated oligonucleotides C1B and G1B with 8mer spacers at the 5′ end were used for immobilization on the sensor surface. M1, M2 and M3 have single base substitutions (in boldface) with respect to C1.

surface and the analyte C is the complementary strand C1 (Table 1). Thus, D is the duplex state after hybridization formed by the interaction of C1 with the unfolded form of G1B (U). In a typical experiment, the sensor surface is stabilized in buffer following immobilization of G1B before the hybridization reaction is initiated by injection of C1. Thus C1, in principle, can hybridize with two components of U: (i) already equilibrated unfolded G1B molecules present on the sensor before injection (U_e) and (ii) G1B molecules unfolding in the presence of C1 (U_t). As a result, theoretically D may be expressed as summation of D_e (duplex formation with U_e) and D_t (duplex formation with U_t). D_e and D_t may be expressed as follows:

$$D_e = \frac{k_a k_u R_{max} C\left(1-e^{-(k_a C+k_d)(t-t_0)}\right)\left(1-e^{-(k_u+k_f)t_e}\right)}{(k_a C+k_d)(k_u+k_f)}, \quad \mathbf{6}$$

$$D_t = \frac{R_{max}\left\{k_f+\left(k_u e^{-(k_u+k_f)t_e}\right)\right\}\left(1-e^{-k_u(t-t_0)}\right)}{(k_u+k_f)}, \quad \mathbf{7}$$

where 't' represents the time elapsed after analyte injection, t_e is the time elapsed before injection (after regeneration), i.e. the pre-equilibration time and t_0 represents time of analyte injection.

Thus, $D = D_e + D_t$ from Equations (6) and (7) can be expressed as follows:

$$D = \frac{k_a k_u R_{max} C\left(1-e^{-(k_a C+k_d)(t-t_0)}\right)\left(1-e^{-(k_u+k_f)t_e}\right)}{(k_a C+k_d)(k_u+k_f)} + \frac{R_{max}\left\{k_f+\left(k_u e^{-(k_u+k_f)t_e}\right)\right\}\left(1-e^{-k_u(t-t_0)}\right)}{(k_u+k_f)} + R_i, \quad \mathbf{8}$$

where R_i is a fitting parameter which is equivalent to any response change owing to the alteration in bulk refractive indices between the running buffer and the analyte injection buffer. The dissociation phase of the sensorgram is fitted according to Equation 3. Thus in a typical experiment, the surface is regenerated (to denature immobilized oligonucleotide) and then equilibrated for a fixed time using running buffer before the analyte is injected in the same buffer. After a defined period of analyte injection, the dissociation phase is monitored. Fitting of the dissociation phase using Equation 3 is done first to obtain k_d, which is used to extract k_a, k_u and k_f from the association phase (Equation 8).

MATERIALS AND METHODS

All oligodeoxynucleotides used in this study (Table 1) were obtained in high-performance liquid chromatography (HPLC) purified form from Sigma Genosys and dissolved in MilliQ purified water. Single strand concentrations of the oligonucleotides were determined using molar extinction coefficient ($\varepsilon_{260nm} = 7913\ M^{-1}\ cm^{-1}$) calculated according to the method of Gray *et al*. (29).

Circular dichroism

Circular dichroism (CD) measurements were performed on a Jasco Spectropolarimeter (model J 715) equipped with a thermostat controlled cell holder with a cell path length of 1 cm as described previously (30). An aliquot of 1.28 μM of G1 in buffer (10 mM HEPES, 150 mM NaCl and 3 mM $MgCl_2$, pH 7.4 adjusted with NaOH) was heated at 95°C for 10 min before slowly cooling to 25°C and mixed with C1 (1.28, 2.56 or 3.84 μM). Samples were equilibrated for at least 2 h after each addition before recording CD spectra from 230 to 330 nm with an averaging time of 3 s.

PAGE

Non-denaturing gel electrophoresis experiments were performed with labeled C1 [5′ end labeled with T4 polynucleotide kinase (New England Biolabs)] and [^{32}P]ATP. Free ATP was removed by denaturing gel electrophoresis. Experiments were done in 10 mM HEPES, 150 mM NaCl and 3 mM $MgCl_2$, pH 7.4 (adjusted with NaOH) using radiolabeled 10 nM C1 (in the presence of 0.5 μM unlabeled C1) after heating at 95°C for 10 min followed by incubation at 4°C for 18 h with G1 (0.5 or 1.5 μM) in the presence or absence (15 min) of DNase I (5 U) before loading on a non-denaturing 20% polyacrylamide gel. Electrophoresis was performed in 0.5× Tris–borate–EDTA (TBE) buffer (pH 8.0) in a thermostated apparatus (SE 600; Hoefer Scientific) run at 4°C for 6–8 h at 90 V. Gels were vacuum dried and analyzed on a phosphorimager (Fujifilm FLA 2000).

Measurement and analysis of hybridization kinetics using surface plasmon resonance

SPR measurements were performed with BIAcore 2000 (BIAcore Inc.) system using streptavidin-coated sensor chips (Sensor chip SA; BIAcore Inc.). The 39mer 5′-biotinylated sequence G1B and C1B were immobilized on flow cells as described previously (31). Flow cell 1 was left blank as control to account for any signal generated owing to bulk solvent effect or any other effect not specific to the DNA interaction, which was subtracted from the signal obtained in flow cell 2 and 3. All experiments were performed at 25°C using running buffer (filtered and degassed 10 mM HEPES with 150 mM of either KCl, NaCl or LiCl and 0.005% surfactant IGEPAL) at pH 7.4 (adjusted with the respective base KOH, NaOH or LiOH, respectively). Oligonucleotide immobilized surface was exposed to the running buffer for at least 2 h at a flow rate of 5 μl/min for attaining base line stability. Analyte (C1, M1, M2, M3 or G1) solutions at different concentrations (16–1024 nM) in the running buffer were injected (at 20 μl/min for 180 s) in random series to avoid any systematic error, using an automated protocol. Following this, dissociation from the surface was monitored for 300 s in

running buffer. Seven different concentrations were used for each analyte and each injection was run in duplicate before fitting to respective equations in order to extract kinetic parameters. Regeneration was done using 1 M NaCl in 50 mM NaOH, as the running buffer could not completely dissociate the complex from the surface. Mass transfer analysis done at varying flow rates (5, 20 and 50 µl/min) showed no significant difference in association rates. The BIAevaluation 3.1.1 software supplied by manufacturer was used to compile the quadruplex-coupled (QC) hybridization model. BIAevaluation 3.1.1 was used as it is for fitting the simple hybridization model. The dissociation phase was used to determine k_d, which was used in the association phase to extract k_f, k_u and k_a (according to the QC model using Equation 8).

RESULTS

Hybridization of the purine-rich strand was influenced by quadruplex formation on sensor surface

Figure 1 shows that the purine-rich strand (G1) from *c-myc* NHE forms parallel G-quadruplex under our experimental conditions as indicated by the characteristic positive and negative maxima at 262 and 236 nm, respectively (16). Many previous reports have observed G-quadruplex formation *in vitro* by this sequence under various conditions (12,13,31–33). Duplex formation was observed on titration with C1 (with 1:1 molar ratio; positive peak shifts to 268 nm); however, no triplex formation [expected positive peak at 282 nm (29)] could be observed on using excess C1. At molar excess of C1, the observed CD profile is characteristic of a mixture of unstructured single strand C1 [positive maxima at 277 nm (14)] and duplex DNA. The reason for not observing any intramolecular C-tetraplex formation (with positive CD peak at 285 nm) at molar excess of C1 may be the slightly acidic conditions required for C-tetraplex formation (14,30).

In a previous study using specific binding of Hoechst 33258 to the *c-myc* G-quadruplex, we obtained evidence of quadruplex formation by G1B on the sensor chip surface (31). Herein, G1B was immobilized on sensor and hybridized with increasing concentration of the complementary strand C1 (or M1, M2 and M3). Sensorgrams obtained on hybridization were fitted with the QC model (Equation 8) to obtain very good fits in both

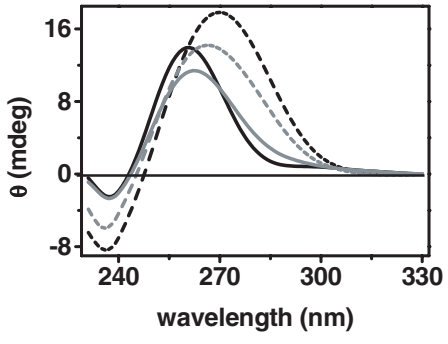

Figure 1. Hybridization of C1 and G1 monitored by CD. An aliquot of 1.28 µM G1 (solid line) was treated with 1.28 µM (gray line), 2.56 µM (gray dashed line) or 3.84 µM (solid dashed line) C1 in 10 mM HEPES, 150 mM NaCl and 3 mM $MgCl_2$, pH 7.4. Spectra were recorded at 25°C, 2 h after each addition.

K^+ and Na^+ (Figure 2a and b, respectively). Results are listed in Table 2. The sensorgrams could not be adequately represented using the two-state association model (Equations 2 and 3). This is evident by a comparison of Figure 2b and c wherein the same set of sensorgrams obtained in Na^+ was fitted using either the QC model or the two-state model, respectively. A similar effect was also observed in K^+ indicating secondary structure formation by the *c-myc* purine-rich sequence on the sensor in both K^+ and Na^+. The complementary pyrimidine-rich strand does not adopt secondary structure at pH 7.4 as seen in Figure 1 with molar excess of C1, as observed earlier (14,30). We used biotinylated C1 (C1B) as a control as it was expected to follow simple two-state hybridization in the absence of additional folding/unfolding equilibrium on sensor like G1B. Figure 2d shows that the sensorgrams obtained with G1 in the mobile phase complied with a two-state hybridization model. Similarly, G-quadruplex formation in the presence of Li^+ is unlikely whereby we expected duplex formation to follow a simple hybridization model. Sensorgrams obtained in 150 mM Li^+ could be fitted satisfactorily without using a QC model (Supplementary Figure 2). Taken together, these observations indicate that the effect of secondary structure formation on hybridization is not an artifact. An 8mer spacer separating biotin from the actual NHE sequence was used such that it tethers off the surface and minimizes the effect of the carboxymethyl dextran surface on the interaction.

Before using the QC model, it was important to ascertain whether, triplex formation was occurring at high analyte concentration as this could contribute to the biphasic transition considered in our model. We did not observe triplex formation by CD (Figure 1). This was further confirmed using a non-denaturing PAGE with labeled C1 in the presence of excess G1, which showed duplex but no triplex formation as confirmed by DNase I cleavage (Figure 2e). Table 2 summarizes the kinetic parameters obtained using the QC model for hybridization with C1 and three other single base mutant oligonucleotides (M1, M2 and M3) in the mobile phase. In case of C1, as expected, the folded form of the G-quadruplex attached to the sensor was more stable in K^+ than Na^+ [as observed from the corresponding folding half-lives ($t_{f1/2}$) and equilibrium folding constants (K_F)] (Table 2). This resulted in a relatively higher amount of unfolded form on the sensor surface in case of Na^+ and was reflected in the increased amount of hybridization observed in Na^+. The equilibrium RU observed in K^+ (Figure 2a) was lower than in Na^+ (Figure 2b) by almost 4-fold as expected from the difference in respective K_F values. Our results are consistent with previous reports indicating stabilizing effect of K^+ on G-quadruplex folding in general (34,35). Similar observations have also been made in the recent study on folding/unfolding of the telomeric G-quadruplex (23). Bimolecular hybridization yielded an equilibrium dissociation constant of 3.61×10^{-10} M in K^+ (and 0.97×10^{-10} M in Na^+), which is of the same order of magnitude as observed by others using SPR under similar conditions (23,36). The observed higher duplex binding affinity in Na^+ with respect to K^+ was primarily due to increased (~3.7-fold) duplex association in the presence of Na^+ as the dissociation constants in both cases were similar. The mutants (M1, M2 and M3) were used to ascertain the QC model as they were expected to change the hybridization rates (k_a/k_d) without affecting the folding/unfolding (k_u/k_f) of G1B. We obtained

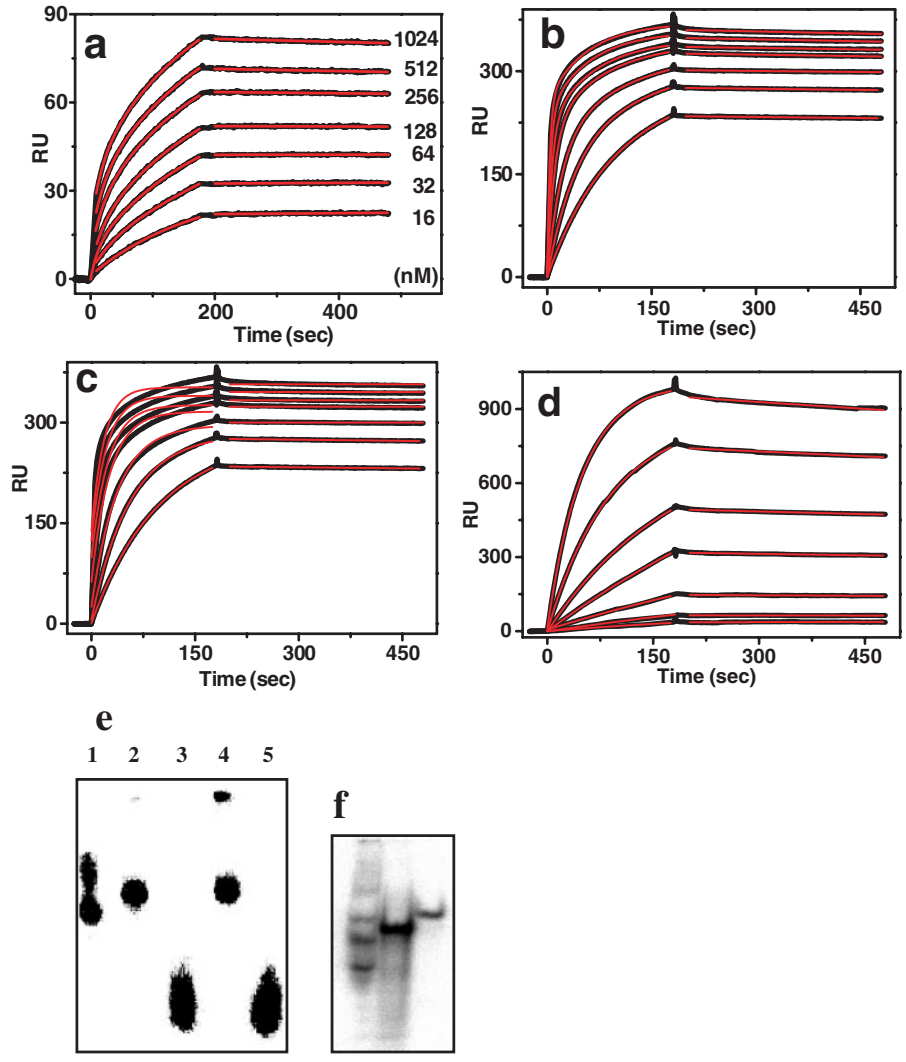

Figure 2. Sensorgrams analyzed with simple versus QC hybridization models. Sensorgrams were obtained by hybridization with immobilized G1B (**a–c**) or C1B (**d**) using 16, 32, 64, 128, 256, 512 or 1024 nM of the respective complementary strand in the mobile phase. Fitted curves (red) were obtained by fitting the sensorgrams (black) with either the QC model using Equation 8 (a and b) or simple hybridization model using Equation 2 (c and d) as in Material and Methods. Sensorgrams were obtained at 25°C and pH 7.4 in either 150 mM KCl (a) or NaCl (b–d). Hybridization of C1 and G1 shows no triplex formation (**e**). Reactions had 10 nM of 5′ end labeled and 0.5 μM unlabeled C1 (lane 1) with either, 0.5 μM G1 (lane 2) and 5 U DNase I (lane 3) or 1.5 μM G1 (lane 4) and 5 U DNase I (lane 5). Samples were incubated at 4°C for 18 h before 15 min DNase I treatment (lanes 3 and 5). G1 shows multiple folded conformations (**f**). An aliquot of 10 nM of 5′ end labeled and 0.5 μM unlabeled G1 (lane 1), C1 (lane 2) and 31mer control dT31 (lane 3) were incubated for 4 h at 25°C before separation. Both (e) and (f) were incubated in 10 mM HEPES, 150 mM NaCl, 3mM $MgCl_2$ and pH 7.4. Bands were separated in a 20% non-denaturing PAGE in 0.5× TBE buffer (pH 8.0) at 4°C for 6 h at 90 V and visualized using autoradiography on phosphorimager (Fujifilm FLA 2000).

very similar k_u and k_f parameters for C1 and the mutants (Table 2). The association rates (k_a) observed for the mutants were lower than C1 while the dissociation rate was observed to be somewhat higher only for M1. This is consistent with earlier reports of hybridization observed by SPR using single base mismatches (37). However, on using G1 in the mobile phase, a two-state hybridization reaction gave k_a and k_d values within 5%. In this case association (k_a) was almost 10-fold lower than association with immobilized G1 and dissociation was ~2.6-fold faster yielding a K_D, which was higher than 40-fold. In accordance with the equilibrium folding constant K_F (0.54) obtained for G1B in Na^+ (on sensor surface), ~65% of the injected G1 concentration, which was expected to be unfolded in solution, was used for fitting. We hypothesized that the observed discrepancy could be due to additional secondary structure formation by G1 that does not participate in the hybridization reaction. In order to confirm this, we performed non-denaturing PAGE and found that G1 formed multiple folded conformations while C1 did not show alternative conformations (Figure 2f).

Simple hybridization with pre-equilibrated unfolded G1B and coupled-hybridization with G1B molecules unfolding during injection can be resolved

G1B molecules attached to sensor surface present two different modes for hybridization; (i) unfolded strand owing to the pre-equilibration phase and (ii) G1B unfolding in the presence of C1 during injection. The latter mode is important in the context of genomic sequences where most transitions are

Table 2. Kinetic parameters for quadruplex folding/unfolding and hybridization of the NHE in the *c-myc* promoter[a]

	150 mM K^+ C1[b]	150 mM Na^+ C1[b]	M1[b]	M2[b]	M3[b]	G1[c]
k_u (s^{-1})	7.90×10^{-3} (±1.52%)	1.56×10^{-2} (±1.52%)	1.49×10^{-2} (±1.98%)	1.50×10^{-2} (±2.90%)	1.47×10^{-2} (±1.61%)	
k_f (s^{-1})	1.65×10^{-2} (±1.84%)	8.34×10^{-3} (±2.25%)	9.60×10^{-3} (±3.03%)	9.41×10^{-3} (±5.04%)	8.21×10^{-3} (±2.44%)	
$t_{f1/2}$ (s)	87.7	45.0	47.9	46.3	48.7	
$t_{u1/2}$ (s)	42.0	83.6	73.2	74.3	84.9	
K_F	2.09	0.54	0.65	0.63	0.57	
k_a (M^{-1} s^{-1})	1.37×10^5 (±1.66%)	5.15×10^5 (±0.87%)	2.80×10^5 (±1.24%)	3.91×10^5 (1.29%)	3.82×10^5 (±0.85%)	3.16×10^4 (±0.68%)
k_d (s^{-1})	4.94×10^{-5} (±3.84%)	4.99×10^{-5} (±1.52%)	7.08×10^{-5} (±1.55%)	5.09×10^{-5} (±3.25%)	2.18×10^{-5} (±4.41%)	13.2×10^5 ± 4.41%)
K_D (M)	3.61×10^{-10}	0.97×10^{-10}	2.53×10^{-10}	1.30×10^{-10}	0.57×10^{-10}	41.7×10^{-10}

[a]Sensorgrams were obtained in 150 mM K^+ or Na^+ at 25°C and fitted to the QC hybridization model. K_F is the equilibrium constant for quadruplex formation calculated from k_f/k_u; K_D denotes the equilibrium dissociation constant for duplex formation, given by k_d/k_a. The half-lives, $t_{f1/2}$ (= ln 2/k_u) and $t_{u1/2}$ (= ln2/k_f) are for the folded and unfolded forms, respectively. Numbers in parentheses are for standard errors.
[b]Sensor surface was immobilized with 1165 RU of the G-rich oligonucleotide G1B before using the respective oligonucleotides C1 (in K^+ or Na^+) or M1, M2 and M3 in Na^+ as analyte in the mobile phase. Kinetic parameters were extracted using the QC model.
[c]Sensor surface was immobilized with 1050 RU of the C-rich oligonucleotide C1B; in accordance with the folding constant K_F (0.54) obtained for G1B (equilibrium on surface) ~65% of the injected G1 concentration, which was expected to be unfolded in solution was used for fitting. Kinetic parameters were extracted using a simple hybridization model (1:1 Langmuir association from BIAevalution 3.1.1).

bound to occur in the presence of the complementary strand. We attempted to resolve these components. Using an association model after incorporating the secondary structure unfolding (QC model) allowed us to simulate the different components of the bimolecular association reaction independently. Figure 3 shows the sensorgrams obtained in Na^+ at increasing C1 concentration (in mobile phase) along with the theoretically obtained simulations (Materials and Methods) for D_e and D_t. Experiments in Na^+ are shown as the higher observed amplitude (equilibrium RU) relative to hybridization in K^+ gives more clarity to our observations; similar results were obtained with K^+ also. D_e denotes duplex formation owing to hybridization of C1 with the pre-existing unfolded G1B (as a result of the quadruplex folding/unfolding equilibrium on sensor surface) and D_t denotes association with G1B molecules, which unfold under the influence of the complementary strand during injection. In all cases, as expected, both components together constitute the fitted curve shown in red. At low strand concentration, hybridization with pre-existing unfolded molecules (D_e) on the sensor surface was slow and the major component of association was apparently from the molecules, which unfold during the injection time (D_t). At higher strand concentrations (>64 nM), we observed a trend reversal—higher component of the association was from a very fast saturating hybridization with pre-equilibrated unfolded oligonucleotides.

These observations can be explained by considering two competing equilibria on the sensor surface, intramolecular quadruplex folding/unfolding (k_u/k_f) and bimolecular hybridization (k_a/k_d). As expected for such a coupled reaction, a plot of k_u (G1B unfolding) and k_{obs} (k_a*C + k_d where C is analyte concentration) of hybridization versus strand concentration (Figure 3g), generated using kinetically extracted parameters, showed that k_u remained constant whereas k_{obs} increased linearly with the concentration of analyte. Thus at low strand concentration, rate of duplex formation was slower. The relatively fast unfolding kinetics in this case contributes more to the overall duplex formation as exemplified by a higher D_t component in Figure 3a–c. On the other hand, it also implies that at low C1 concentration the association reaction would follow a simple 1:1 Langmuir model as hybridization is the rate-limiting step. We tested this possibility using very low C1 concentration (1–16 nM) and all the sensorgrams could be fitted using simple association kinetics (Supplementary Figure 3), without considering the coupled model. With increase in strand concentration, rate of hybridization increases and duplex formation with the pre-equilibrated unfolded form (D_e) was predominant (Figures 3d–f). A sharp transition between D_e and D_t profiles was observed >64 nM (Figure 3c). This is shown in Figure 3h, where the contribution of D_e and D_t components as a percentage of total duplex formation was plotted versus strand concentration.

G-quadruplex formation is kinetically favored at low complementary strand concentration

It was observed that the promoter element regulating *c-myc* is sensitive to S1 nuclease cleavage designating it a NHE III_1 (8,38). It has been speculated that G-quadruplex formation in this region might be the reason for nuclease sensitivity (13). Using our model we attempted to explore whether the existence of a G-quadruplex was kinetically feasible. Figure 3g and h together indicated a change in the rate-determining step in the range of 30–100 nM C1 concentration suggesting that <100 nM, duplex formation was kinetically unfavorable. An estimate of the concentration of immobilized G1B indicates it to be ~82.6 nM (surface concentration calculation was performed assuming monolayer formation on sensor and is given in Supplementary Material). This suggests that the cross-over in the rate-determining step occurred in the region of equimolar strand concentration.

DISCUSSION

Recent evidence directly implicates quadruplexes in various biological processes including regulation of the oncogene

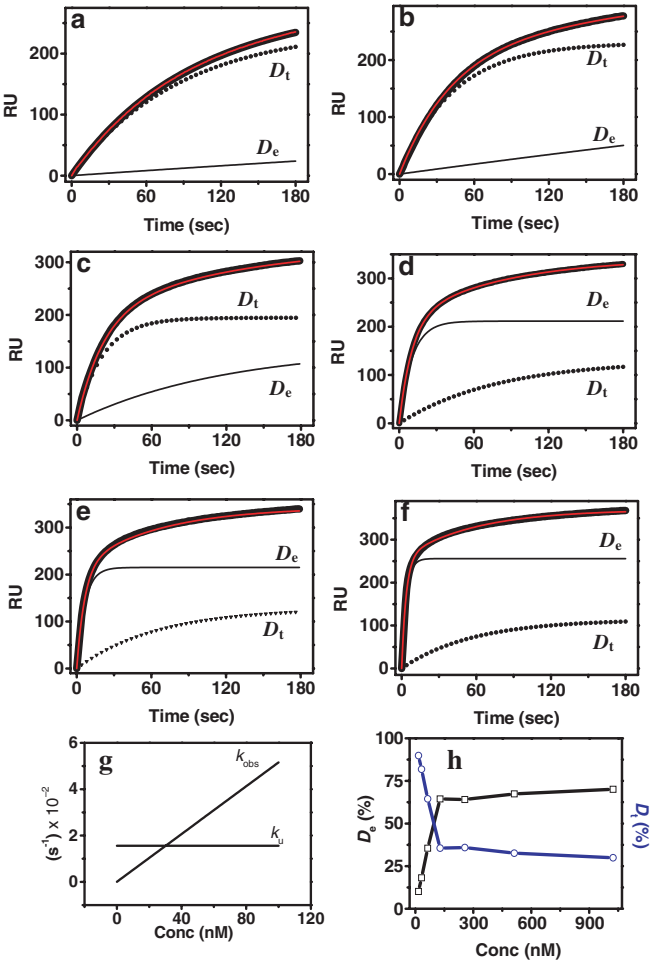

Figure 3. Resolution of two modes of duplex formation on sensor surface using QC hybridization model. Folding/unfolding equilibrium of quadruplex molecules on sensor surface present pre-equilibrated unfolded molecules as well as molecules unfolding during injection, for hybridization. QC hybridization model has been used to separate these components. Sensorgrams obtained with immobilized G1B and 16 (**a**), 32 (**b**), 64 (**c**), 128 (**d**), 256 (**e**) and 1024 (**f**) nM C1 are shown in black. Simulated curves for hybridization with pre-equilibrated unfolded G1B (D_e) and unfolding G1B during injection (D_t) were generated using Equations 6 and 7, respectively, and are marked in the figures. The theoretically derived hybridization curve is shown in red and is the sum of D_e and D_t in all cases. The dependence of the unfolding rate constant (k_u) and k_{obs} for hybridization on strand concentration using the kinetically extracted parameters obtained form QC model is shown in (**g**). Relationship between D_e and D_t, as percentage contribution towards total duplex formation as a function of strand concentration is shown in (**h**). All experiments were done in 150 mM NaCl as described in Figure 2.

c-myc (12,13,19,20,32–39). We recently observed that mutations, which increase the *c-myc* expression, affect the quadruplex/duplex competition in the promoter region of *c-myc* by enhancing duplex formation *in vitro* (40). However, though many reports have studied thermodynamics of quadruplex formation only a few have studied the kinetics (22,23). In a biological context, it would be of interest to observe both folding/unfolding of quadruplex and hybridization simultaneously, in the presence of low and equimolar concentration of both strands. Here, we report the development of an SPR-based method, which allows the resolution of two simultaneous and competing equilibria at very low concentrations. Using the sequence from the NHE III_1 in the promoter region of *c-myc* we demonstrate that at low equimolar strand concentration duplex formation is unfavorable.

While this work was in progress, a coupled-hybridization model was reported, which studied folding versus hybridization of the quadruplex formed by the telomeric repeat $(TTAGGG)_4$ (23). They observed using a series of concentrations that simple two-state hybridization could not simulate the observed sensorgrams when the immobilized molecules could adopt secondary structure, indicating the presence of an additional equilibrium. However, the possibility of a second equilibrium arising out of triplex formation at high analyte strand concentration, which could contribute to a non-two-state model was not ruled out. The authors applied their model to equilibrium conditions and showed that at low and equimolar strand concentration quadruplex formation is favored over hybridization. We have used an alternative approach from first principles to derive a QC model and applied this to demonstrate that quadruplex–duplex competition can be observed without considering the equilibrium approximations or the equimolar conditions (Figure 3), as performed in the previous study. Our general solution clearly shows that quadruplex–duplex competition can be controlled by complementary strand concentration, which changes the rate-determining step involved in quadruplex folding vis-à-vis hybridization. This results in a mechanistic change with increasing complementary strand concentration and the 'cross-over' region is at near equimolar concentration. A discussion comparing the two methods is given in Supplementary Material.

The quadruplex folding/unfolding constants obtained by us are within the same order of magnitude as observed before for telomeric sequences from human (22,23) and *Oxytricha* (41) (Table 3). It was interesting to note that in the presence of K^+, half-life of folded *c-myc* quadruplex ($t_{f1/2} = 87.7$ s) was 6-fold less than that of the telomeric sequence ($t_{f1/2} = 533$ s) (23), suggesting that the *c-myc* quadruplex was thermodynamically unfavorable relative to the telomeric quadruplex. This is interesting, considering the fact that the number of G-tetrad units (which are believed to impart stability to the quadruplex moiety) are three in the telomeric quadruplex in comparison to four possible in the *c-myc* quadruplex. Thus factors other than tetrad stability, e.g. loop constitution, may be important in rendering stability to the quadruplex moiety (34).

We also noted the hybridization rates observed for several sequences using SPR and compared them with the ones obtained by our 31mer sequence (Table 3). The association constant reported by Zhao *et al.* (23), for the telomere sequence studied under analogous conditions (K^+) was higher by an order of magnitude. The reason for this substantial difference is not very clear to us. However, some discrepancy may result in the comparison of the parameters as ~75% standard error was associated with the fitted dissociation constant, which was used for fitting the association curve in the sensorgram, in the previous study (23). In an earlier study (40), we determined hybridization constants for G1 and C1 at pH 6.6 and obtained k_a of $3.2 \times 10^4\ M^{-1}\ s^{-1}$ and k_d of $3.5 \times 10^{-3}\ s^{-1}$, which were an order of magnitude different from the ones observed here. A difference in terms of lower rates is expected at pH 6.6 relative to pH 7.4. However, the QC model was not considered in the earlier case, which may be the reason for observed errors in fitting (16–23%) and the large difference

Table 3. Comparison of kinetic parameters obtained for G-quadruplex folding/unfolding and duplex formation by SPR and other methods

Sequence	G-quadruplex folding		Hybridization			Method	Reference
	k_u (s^{-1})	k_f (s^{-1})	k_a (M^{-1} s^{-1})	k_d (s^{-1})	K_D (M)		
$(G_3TTA)_3G_3$[a]	6.0×10^{-3}	2.4×10^{-2}				FRET	(22)
$(T_4G_4)_4$[b]	$\sim 10^{-5}$	1.7×10^{-3}				PAGE	(38)
TAGTTGTGACGTACA[c]			12.0×10^{3}	2.9×10^{-4}	2.5×10^{-8}	SPR	(39)
$(TTAGGG)_4$[d]	1.3×10^{-3}	1.2×10^{-2}	1.3×10^{6}	1.6×10^{-5}[e]	7.8×10^{-10}	SPR	(23)
$(G_4AG_3T)_2G_4AAGGTG_4$[d]	7.9×10^{-3}	1.6×10^{-2}	1.4×10^{5}	5.0×10^{-5}	3.6×10^{-10}	SPR	This study

[a]k_u was calculated from experimentally determined rate constant of folding k_f (by FRET) and equilibrium constant K_F (determined by UV-melting) in 100 mM Na^+ at 37°C.
[b]In 50 mM Na^+ at 37°C.
[c]In 150 mM Na^+ at 20°C.
[d]In 150 mM K^+ at 25°C.
[e]Standard error of ~75% reported. Blank spaces indicated that the parameters were not determined.

in rates observed in comparison with the current study. Several previous reports have determined folding/unfolding constants (K_F) of quadruplexes by UV-melting and compared or used them for extraction of other kinetic parameters (22,23,37). The high melting point of G1 under our conditions [>92°C (K. Halder and S. Chowdhury, unpublished data)] precluded this.

It must be noted that multiple folding/unfolding rates may result from the presence of more than one folded motif on the sensor surface (as evident from Figure 2f). Therefore, the reported kinetic folding/unfolding parameters are likely to represent average apparent values. One of the limitations of fitting multiple parameters to a single equation (Equation 8) is that it could potentially give several minima, i.e. several sets of optimal values for the parameters, which equally fit the equation. While such a possibility cannot be completely ruled out, typically, in such cases when optimization of all parameters is carried out simultaneously, large standard deviations result. We further checked the effect of each parameter on the fitting by perturbing (both increase and decrease) each parameter at a time and observed its effect on the other variables. Chi-square values were observed to progressively increase indicating deviation from the correct solution in all cases (Supplementary Table 1). Additionally, in our case all folded forms are likely to result from the parallel form of the motif (as observed in the CD spectra in Figure 1 and high T_M in UV-melting experiments). Therefore, the difference between individual kinetic rates may not be too high, which may be a reason for observed low standard errors for the parameters.

Our analysis with the *c-myc* sequence suggests that at the low intracellular concentrations [$<10^{-11}$ M (23)], the chances of favorable quadruplex formation cannot be ruled out though it is thermodynamically more expensive than duplex formation. This is interesting in the context of previous reports, which have observed that the promoter element of *c-myc* harboring this sequence exists in a strand-separated form *in vivo* and has been designated as a NHE for this reason (8,38). However, it may not be true for all potential quadruplex-forming sequences as the stability of the motif (k_u/k_f equilibrium) will play a significant role in the competition. Analytical component resolution (D_e and D_t modes of hybridization, Figure 3) is important with respect to chromosomal sequence where unfolding of the quadruplex is mostly in presence of the complementary strand, which is represented by the D_t component. Thus D_t is expected to more appropriately represent *in vivo* situations allowing extrapolations from *in vitro* studies whereby D_t may be used to examine the effect of ligands and other factors on the structural transitions in the context of triplex formation or G-quadruplex stabilizing molecules. However, it must be noted that the short immobilized oligonucleotide on the sensor surface and the complementary strand in the mobile phase do not effectively replicate an *in vivo* situation wherein the duplex state of the flanking regions are bound to have an effect on the kinetic parameters. It may be contemplated that a 'zipping-like' mechanism may help duplex formation. However, intracellular molecules may help in the stabilization of the quadruplex.

Proposed models of NHE III_1 controlled *c-myc* expression invoke G-quadruplex formation in the NHE as a negative regulator (13,33). This is primarily based on observations that a single base mutation, which destabilizes the quadruplex, increases *c-myc* expression while stabilization of the motif decreases *c-myc* expression (13). The paranemic quadruplex form is converted to unstructured single strand form before *c-myc* activation—possibly by intervention of the transcription factor NM23-H2 (11), which may bind to both forms of the NHE. CNBP and hnRNP K are also known to play a role in *c-myc* transcriptional activation by binding to the purine- and pyrimidine-rich strands of the duplex NHE directly (9,42,43). These collectively suggest that both the folded and the unfolded form of the NHE are significant components of *c-myc* transcription control, which may be orchestrated by presentation of different molecular topology as transcription factor binding sites. The intrinsic properties of these topologies conferring different molecular recognition properties vis-à-vis duplex DNA make them attractive targets for selectively intervening oncogene expression. In addition to *c-myc*, presence of potential quadruplex forming elements in the promoters of various other genes including PDGF-A, Ki-ras, c-myb, c-vav and c-rel (A. Verma and S. Chowdhury, unpublished data) suggest a method of expression control in genes controlling growth and proliferation, which is mediated by interconversion between the duplex and the quadruplex forms.

SUPPLEMENTARY MATERIAL

Supplementary Material is available at NAR Online.

ACKNOWLEDGEMENTS

We wish to thank Dr Swapan K. Das, IGIB and Dr Raimundo Gargallo, University of Barcelona, Spain for helpful

discussions and Dr Munia Ganguli (IGIB) for carefully editing the manuscript. We also wish to thank reviewer for helping us in enriching the content of the manuscript. S.C. acknowledges Prof. S. K. Brahmachari for constant support and CSIR for research grant. K.H. acknowledges research fellowship from CSIR. Funding to pay the Open Access publication charges for this article were waived by Oxford University Press.

Conflict of interest statement. None declared.

REFERENCES

1. Pelengaris,S., Rudolph,B. and Littlewood,T. (2000) Action of Myc *in vivo*—proliferation and apoptosis. *Curr. Opin. Genet. Dev.*, **10**, 100–105.
2. Spencer,C.A. and Groudine,M. (1991) Control of c-myc regulation in normal and neoplastic cells. *Adv. Cancer Res.*, **56**, 1–48.
3. Facchini,L.M. and Penn,L.Z. (1998) The molecular role of Myc in growth and transformation: recent discoveries lead to new insights. *FASEB J.*, **12**, 633–651.
4. Marcu,K.B., Bossone,S.A. and Patel,A.J. (1992) myc function and regulation. *Annu. Rev. Biochem.*, **61**, 809–860.
5. Adachi,S., Obaya,A.J., Han,Z., Ramos-Desimone,N., Wyche,J.H. and Sedivy,J.M. (2001) c-Myc is necessary for DNA damage-induced apoptosis in the G_2 phase of the cell cycle. *Mol. Cell. Biol.*, **21**, 4929–4937.
6. Canelles,M., Delgado,M.D., Hyland,K.M., Lerga,A., Richard,C., Dang,C.V. and Leon,J. (1997) Max and inhibitory c-Myc mutants induce erythroid differentiation and resistance to apoptosis in human myeloid leukemia cells. *Oncogene*, **14**, 1315–1327.
7. Levens,D., Duncan,R.C., Tomonaga,T., Michelotti,G.A., Collins,I., Davis-Smyth,T., Zheng,T. and Michelotti,E.F. (1997) DNA conformation, topology, and the regulation of c-myc expression. *Curr. Top. Microbiol. Immunol.*, **224**, 33–46.
8. Siebenlist,U., Hennighausen,L., Battey,J. and Leder,P. (1984) Chromatin structure and protein binding in the putative regulatory region of the *c-myc* gene in Burkitt lymphoma. *Cell*, **37**, 381–391.
9. Tomonaga,T. and Levens,D. (1996) Activating transcription from single stranded DNA. *Proc. Natl Acad. Sci. USA*, **93**, 5830–5835.
10. Cooney,M., Czernuszewicz,G., Postel,E.H., Flint,S.J. and Hogan,M.E. (1988) Site-specific oligonucleotide binding represses transcription of the human *c-myc* gene *in vitro*. *Science*, **241**, 456–459.
11. Postel,E.H., Berberich,S.J., Rooney,J.W. and Kaetzel,D.M. (2000) Human NM23/nucleoside diphosphate kinase regulates gene expression through DNA binding to nuclease-hypersensitive transcriptional elements. *J Bioenerg. Biomembr.*, **32**, 277–284.
12. Simonsson,T., Pecinka,P. and Kubista,M. (1998) DNA tetraplex formation in the control region of c-myc. *Nucleic Acids Res.*, **26**, 1167–1172.
13. Siddiqui-Jain,A., Grand,C.L., Bearss,D.J. and Hurley,L.H. (2002) Direct evidence for a G-quadruplex in a promoter region and its targeting with a small molecule to repress c-MYC transcription. *Proc. Natl Acad. Sci. USA*, **99**, 11593–11598.
14. Simonsson,T., Pribylova,M. and Vorlickova,M. (2000) A nuclease hypersensitive element in the human c-myc promoter adopts several distinct i-tetraplex structures. *Biochem. Biophys. Res. Commun.*, **278**, 158–166.
15. Guschlbauer,W., Chantot,J.F. and Thiele,D. (1990) Four-stranded nucleic acid structures 25 years later: from guanosine gels to telomer DNA. *J. Biomol. Struct. Dyn.*, **8**, 491–511.
16. Balagurumoorthy,P. and Brahmachari,S.K. (1994) Structure and stability of human telomeric sequence. *J. Biol. Chem.*, **269**, 21858–21869.
17. Blackburn,E.H. (1991) Structure and function of telomeres. *Nature*, **350**, 569–573.
18. Prochownik,E.V., Kukowska,J. and Rodgers,C. (1988) c-myc antisense transcripts accelerate differentiation and inhibit G1 progression in murine erythroleukemia cells. *Mol. Cell. Biol.*, **8**, 3683–3695.
19. Jinks-Robertson,S. (2002) The genome's best friend. *Nature Genet.*, **31**, 331–332.
20. Cheung,I., Schertzer,M., Rose,A. and Lansdorp,P.M. (2002) Disruption of dog-1 in *Caenorhabditis elegans* triggers deletions upstream of guanine-rich DNA. *Nature Genet.*, **31**, 405–409.
21. Alberti,P. and Mergny,J.L. (2003) DNA duplex-quadruplex exchange as the basis for a nanomolecular machine. *Proc. Natl Acad. Sci. USA*, **100**, 1569–1573.
22. Green,J.J., Ying,L., Klenerman,D. and Balasubramanian,S. (2003) Kinetics of unfolding the human telomeric DNA quadruplex using a PNA trap. *J. Am. Chem. Soc.*, **125**, 3763–3767.
23. Zhao,Y., Kan,Z.Y., Zeng,Z.X., Hao,Y.H., Chen,H. and Tan,Z. (2004) Determining the folding and unfolding rate constants of nucleic acids by biosensor. Application to telomere G-quadruplex. *J. Am. Chem. Soc.*, **126**, 13255–13264.
24. Fivash,M., Towler,E.M. and Fisher,R.J. (1998) BIAcore for macromolecular interaction. *Curr. Opin. Biotechnol.*, **9**, 97–101.
25. Raghavan,M. and Bjorkman,P.J. (1995) BIAcore: a microchip-based system for analyzing the formation of macromolecular complexes. *Structure*, **3**, 331–333.
26. Karlsson,R., Michaelsson,A. and Mattsson,L. (1991) Kinetic analysis of monoclonal antibody–antigen interactions with a new biosensor based analytical system. *J. Immunol. Methods*, **145**, 229–240.
27. Myszka,D.G. (2000) Kinetic, equilibrium, and thermodynamic analysis of macromolecular interactions with BIACORE. *Methods Enzymol.*, **323**, 325–340.
28. O'Shannessy,D.J., Brigham-Burke,M., Soneson,K.K., Hensley,P. and Brooks,I. (1993) Determination of rate and equilibrium binding constants for macromolecular interactions using surface plasmon resonance: use of nonlinear least squares analysis methods. *Anal. Biochem.*, **212**, 457–468.
29. Gray,D.M., Hung,S.H. and Johnson,K.H. (1995) Absorption and circular dichroism spectroscopy of nucleic acid duplexes and triplexes. *Methods Enzymol.*, **246**, 19–34.
30. Mathur,V., Verma,A., Maiti,S. and Chowdhury,S. (2004) Thermodynamics of i-tetraplex formation in the nuclease hypersensitive element of human c-myc promoter. *Biochem. Biophys. Res. Commun.*, **320**, 1220–1227.
31. Maiti,S., Chaudhury,N.K. and Chowdhury,S. (2003) Hoechst 33258 binds to G-quadruplex in the promoter region of human c-myc. *Biochem. Biophys. Res. Commun.*, **310**, 505–512.
32. Phan,A.T., Modi,Y.S. and Patel,D.J. (2004) Propeller-type parallel-stranded G-quadruplexes in the human c-myc promoter. *J. Am. Chem. Soc.*, **126**, 8710–8716.
33. Seenisamy,J., Rezler,E.M., Powell,T.J., Tye,D., Gokhale,V., Joshi,C.S., Siddiqui-Jain,A. and Hurley,L.H. (2004) The dynamic character of the G-quadruplex element in the c-MYC promoter and modification by TMPyP4. *J. Am. Chem. Soc.*, **126**, 8702–8709.
34. Hazel,P., Huppert,J., Balasubramanian,S. and Neidle,S. (2004) Loop-length-dependent folding of G-quadruplexes. *J. Am. Chem. Soc.*, **126**, 16405–16415.
35. Risitano,A. and Fox,K.R. (2003) Stability of intramolecular DNA quadruplexes: comparison with DNA duplexes. *Biochemistry*, **42**, 6507–6513.
36. Gotoh,M., Hasegawa,Y., Shinohara,Y., Shimizu,M. and Tosu,M. (1995) A new approach to determine the effect of mismatches on kinetic parameters in DNA hybridization using an optical biosensor. *DNA Res.*, **2**, 285–293.
37. Jensen,K.K., Orum,H., Nielsen,P.E. and Norden,B. (1997) Kinetics for hybridization of peptide nucleic acids (PNA) with DNA and RNA studied with the BIAcore technique. *Biochemistry*, **36**, 5072–5077.
38. Boles,T.C. and Hogan,M.E. (1987) DNA structure equilibria in the human c-myc gene. *Biochemistry*, **26**, 367–376.
39. Bacolla,A. and Wells,R.D. (2004) Non-B DNA conformations, genomic rearrangements, and human disease. *J. Biol. Chem.*, **279**, 47411–47414.
40. Halder,K., Mathur,V., Chugh,D., Verma,A. and Chowdhury,S. (2005) Quadruplex-Duplex competition in the Nuclease Hypersensitive Element of Human *c-myc* Promoter: C to T mutation in C-rich strand enhances Duplex Association. *Biochem. Biophys. Res. Comm.*, **327**, 49–56.
41. Raghuraman,M.K. and Cech,T.R. (1990) Effect of monovalent cation-induced telomeric DNA structure on the binding of Oxytricha telomeric protein. *Nucleic Acids Res.*, **18**, 4543–4552.
42. Bossone,S.A., Asselin,C., Patel,A.J. and Marcu,K.B. (1992) MAZ, a zinc finger protein, binds to c-MYC and C2 gene sequences regulating transcriptional initiation and termination. *Proc. Natl Acad. Sci. USA*, **89**, 7452–7456.
43. Michelotti,E.F., Tomonaga,T., Krutzsch,H. and Levens,D. (1995) Cellular nucleic acid binding protein regulates the CT element of the human c-myc protooncogene. *J. Biol. Chem.*, **270**, 9494–9499.